Phosphorescent Polymeric Thermometers for In Vitro and In Vivo Temperature Sensing with Minimized Background Interference

Zejing Chen, Kenneth Yin Zhang, Xiao Tong, Yahong Liu, Changyong Hu, Shujuan Liu, Qi Yu, Qiang Zhao, and Wei Huang**

Temperature plays a crucial role in many biological processes. Accurate temperature determination is important for diagnosis and treatment of diseases. Autofluorescence is an unavoidable interference in luminescent bioimaging. Hence, a large amount of research works has been devoted to reducing background autofluorescence and improving signal-to-noise ratio (SNR) in biodetection. Herein, a dual-emissive phosphorescent polymeric thermometer has been developed by incorporating two long-lived phosphorescent iridium(III) complexes into an acrylamide-based thermosensitive polymer. Upon increasing temperature, this polymer undergoes coil-globule transition, which leads to a decrease in polarity of the microenvironment surrounding the iridium(III) complexes and hence brings about emission enhancement of both complexes. Owing to their different sensitivity to surrounding environment, the emission intensity ratio of the two complexes is correlated to the temperature. Thus, the polymer has been used for temperature determination in vitro and in vivo via ratiometric luminescence imaging. More importantly, by using the long-lived phosphorescence of the polymer, temperature mapping in zebrafish has been demonstrated successfully with minimized autofluorescence interference and improved SNR via time-resolved luminescence imaging. To the best of our knowledge, this is the first example to use photoluminescent thermometer for in vivo temperature sensing.

1. Introduction

As a fundamental physical parameter, temperature plays a key role in various physical and chemical processes, and exquisitely affects many physiological activities, such as enzyme reaction, gene expression, cell division, and metabolism.[1] In pathological studies, some malignant cells within tissues are found to maintain higher temperatures than healthy cells owing to abnormal metabolic rates.[2] Hence, accurate measurement of the temperature in living cells and real-time temperature mapping within whole living organism are important in understanding physiological events and contribute to advancements in diagnoses and therapies.[3] Traditional methods based on thermocouple thermometers exhibit low spatial resolution and usually cause organism damage. Luminescent materials including organic dyes,[4] polymers,[5] quantum dots,[6] nanoclusters,[7] upconverting nanoparticles,[8] and proteins[9] have been proposed to address the need. These luminescent probes displayed significant changes in their photophysical properties in response to temperature variation, providing non-invasive and inherently parallel approach that is particularly suitable for intracellular temperature determination.[5a,10]

In most cases, the emission intensity of the photoluminescent thermometer is correlated to the temperature, and hence it appears simple and straightforward to determine the temperature by measuring the intensity.[11] Compared to the intensity-based method, wavelength-ratiometric probes display profile changes in their emission spectra upon temperature variation and the ratio of intensities at two emission wavelengths is used to reflect the temperature, which allows self-calibration and improves accuracy and precision.[4c,5d–f,12] When the probes are applied to in vivo measurements, the luminescence intensity is interfered with autofluorescence generated from endogenous fluorophores, limiting the applications of either intensity-based or wavelength-ratiometric methods.

Z. Chen, Dr. K. Y. Zhang, X. Tong, Y. Liu, C. Hu, Prof. S. Liu, Q. Yu, Prof. Q. Zhao, Prof. W. Huang
Key Laboratory for Organic Electronics and Information Displays and Institute of Advanced Materials (IAM)
Jiangsu National Synergetic Innovation Center for Advanced Materials (SICAM)
Nanjing University of Posts and Telecommunications (NUPT)
Nanjing 210023, P. R. China
E-mail: iamqzhao@njupt.edu.cn; wei-huang@njtech.edu.cn
Prof. W. Huang
Key Laboratory of Flexible Electronics (KLOFE) and Institute of Advanced Materials (IAM)
Jiangsu National Synergetic Innovation Center for Advanced Materials (SICAM)
Nanjing Tech University (NanjingTech)
Nanjing 211816, P. R. China

DOI: 10.1002/adfm.201600706

Time-resolved luminescence imaging,[13] such as photoluminescence lifetime imaging microscopy (PLIM) and time-gated luminescence imaging (TGLI), provides a possibility to analyze emission signals in the time domain even though they occur at the same wavelength. Transition-metal complexes display phosphorescence which shows remarkably longer lifetimes than autofluorescence. Additionally, these complexes exhibit high quantum efficiency, significant Stokes shift, and excellent photostability.[14] Especially, their phosphorescence properties come from various charge-transfer states, which are sensitive to surrounding environments, including temperature. These characteristics render them good candidates for bioimaging of temperature.

In this work, we designed and synthesized two phosphorescent polymeric thermometers (**P1** and **P2**, **Scheme 1**) by incorporating phosphorescent iridium(III) complexes into water-soluble acrylamide-based thermosensitive polymers. The phosphorescent polymers **P1** and **P2** showed orange and cyan emission, respectively, which were significantly enhanced upon increasing temperature from 16 to 40 °C because the polymers underwent conformational changes from an extended structure to an aggregated state, leading to an increase in rigidity and a decrease in polarity of the microenvironment of the iridium(III) complexes thus bringing about emission enhancement. Interestingly, the sensitivities of the thermometers are quite different. Therefore, a polymer involving both the orange- and cyan-emissive iridium(III) complexes was synthesized as wavelength-ratiometric thermometer (Scheme 1). This dual-emissive phosphorescent polymeric thermometer (**P3**) has been used for in vitro and in vivo temperature measurement via ratiometric photoluminescence imaging and time-resolved luminescence imaging. Importantly, the long-lived phosphorescence of **P3** has been easily distinguished from short-lived autofluorescence in the zebrafish imaging. To the best of our knowledge, this is the first report of using photoluminescent thermometer for in vivo temperature mapping.

2. Result and Discussion

2.1. Design, Synthesis, and Characterization of Polymers

Poly *N*-n-propylacrylamide (PNNPAM) was selected as the thermosensitive polymer backbone since it undergoes a reversible lower critical solution temperature phase transition between a swollen hydrated state and a shrunken dehydrated state in the temperature range of about 20 to 40 °C,[5c,15] which covers the physiological temperature of humans and most animals. To guarantee the polymers having enough thermosensitivity, the PNNPAM units in polymers were controlled above 96 mol%. Around 2% of the monomers with a cationic ammonium were introduced into PNNPAM to improve water solubility and cellular uptake.[5c,15c] Owing to the sensitive phosphorescence properties to the microenvironment, two iridium(III) complexes **Ir1** and **Ir2** (Scheme 1), which displayed orange and cyan phosphorescence, respectively, were selected to convert the temperature-induced conformational change of PNNPAM into photoluminescence signals, facilitating the visualization

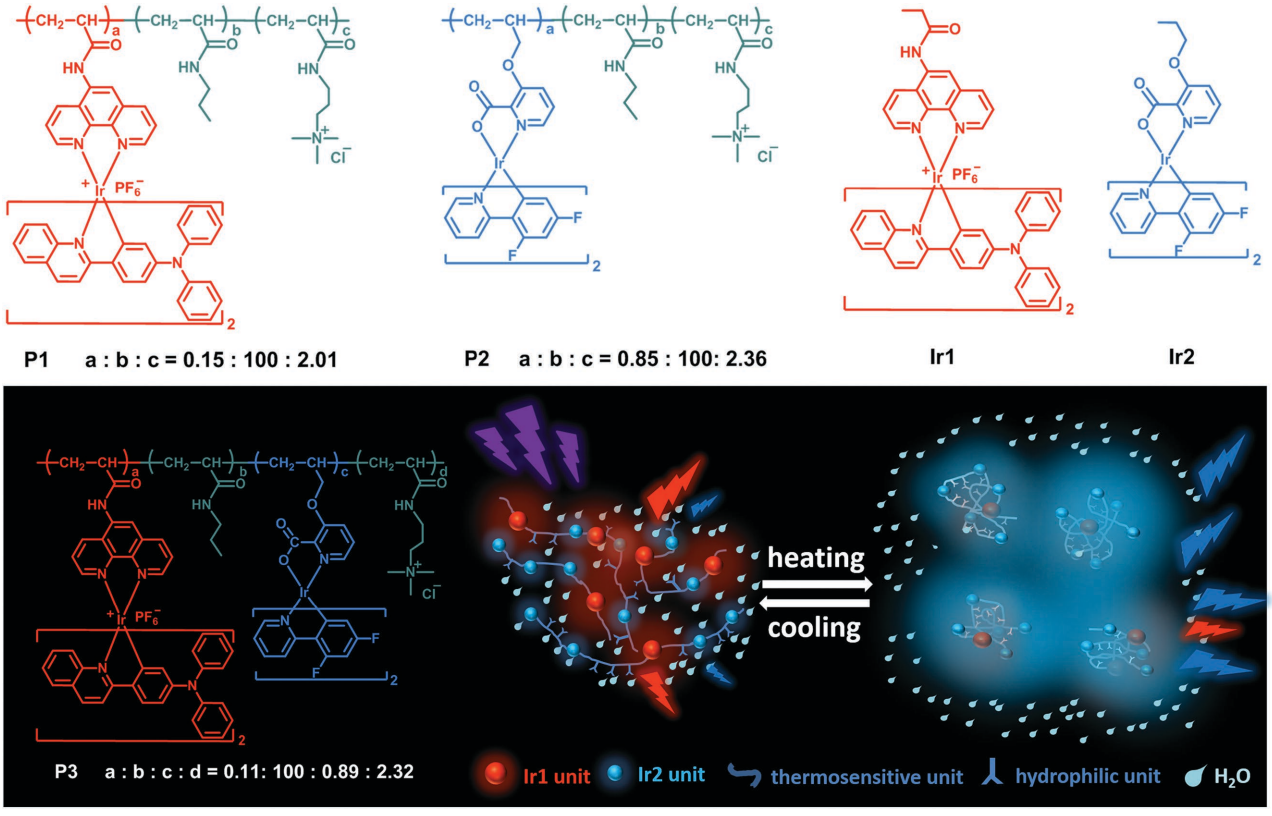

Scheme 1. Schematic diagram and chemical structures of polymers (**P1**, **P2**, and **P3**) and iridium(III) complexes (**Ir1** and **Ir2**).

Adv. Funct. Mater. **2016**,
DOI: 10.1002/adfm.201600706

by naked eyes and the detection via photoluminescence microscopy.

The synthetic routes and chemical structures of complexes and polymers were shown in Scheme S1–S3 (Supporting Information). For complexes **Ir1** and **Ir3**, the cyclometalated ligand (*N,N*-diphenyl-4-(quinolin-2-yl)aniline (pqa), H*C^N* ligand) was easily obtained in good yield by a Friedländer condensation reaction of 2-aminobenzaldehyde with 1-(4-(diphenylamino)phenyl)-ethanone according to a previously published procedure.[16a] And the cyclometalated iridium(III)-chlorobridged dimers of a general formula $(C^N)_2Ir(\mu\text{-}Cl)_2Ir(C^N)_2$ were synthesized according to the Nonoyama route by refluxing $IrCl_3{\cdot}3H_2O$ with 2.0–2.5 equiv. of cyclometalated ligand (H*C^N*) in a 3:1 (V:V) mixture of 2-ethoxyethanol and water.[16b–d] Then, the complexes were synthesized through the bridge-splitting reaction of $[Ir(pqa)_2Cl]_2$ (pqa =*N,N*-diphenyl-4-(quinolin-2-yl)aniline) and subsequent complexation with the ligand *N*-(1,10-phenanthrolin-5-yl)propionamide (pap) and *N*-(1,10-phenanthrolin-5-yl) acrylamide (paa), respectively, which were synthesized through amidation of 1,10-phenanthrolin-5-amine with the propionyl chloride or acryloyl chloride. As for complexes **Ir2** and **Ir4**, they were obtained via the reaction of 1-bromopropane or 3-bromoprop-1-ene with the precursor complex **15**, respectively, which was prepared according to a previously reported procedure.[16e] Finally, the target copolymer **P1** or **P2** was synthesized via free radical polymerization from **Ir3** or **Ir4**, PNNPAM and (3-acrylamidopropyl)trimethylammonium. Polymer **P3** containing both the **Ir1** and **Ir2** units was also prepared using the same method. All of the complexes and copolymers were obtained as powders and they were characterized by NMR. The number-average molecular weight of these polymers are 11 200, 10 300, and 10 100 with polydispersity indexes (PDI) of 1.83, 2.03, and 2.05, respectively, which were measured via gel permeation chromatography (GPC) in tetrahydrofuran (THF) by using the calibration curve of polystyrene standards (**Table 1**). The actual contents of complexes in polymers are different from the initial feed ratio, which is due to the reaction activity or steric hindrance of complexes.

The photoluminescence (PL) spectra of copolymers in a phosphate buffer solution were shown in **Figure 1**, which are corresponding to the emission spectra of complexes **Ir1** and **Ir2** (Figure S1, Supporting Information). Upon photoexcitation, **P1** showed a broad emission band centered at 590 nm, while **P2** displayed a structured emission band with the maxima at 470 and 490 nm. Generally, the PL spectra from the ligand-centered $^3\pi$–π^* state display vibronic progressions, whereas those from the charge-transfer (CT) state are broad and featureless. Thus, the emissions of **P1** and **P2** have been assigned to metal-to-ligand charge-transfer (^{3}MLCT) and triplet intraligand (^{3}IL) excited states, respectively. It is noteworthy that **P1** and **P2** could be simultaneously excited at 405 nm, which is one of the most commonly used laser sources in confocal microscopy, and that their respective orange and cyan phosphorescences were spectrally well separated (Δ > 100 nm). Additionally, both emission bands of **P3** basically retained their characteristics indicating limited energy or electron transfer between these two complexes units. Last but equally important is that the quantum yields of **P1**, **P2** and **P3** in aqueous solution were 0.12, 0.10, and 0.12, respectively (Table S1, Supporting Information), which could support the highly resolved luminescence images.

2.2. Photoluminescence Responses of Polymers to Temperature Change

The photoluminescence response of **P1** and **P2** to temperature has been investigated via emission spectral change (**Figure 2**a,b). Upon increasing temperature from 16 to 36 °C, both **P1** and **P2** displayed emission enhancement owing to the increase in rigidity and decrease in polarity of the microenvironment of the iridium(III) complex units, which were brought about by the conformational change of the polymer backbones.[5d,14b,17] Very interestingly, the emission enhancement factors of the polymeric thermometers were different; the photoluminescence of **P2** at 470 nm was enhanced by 8.6-fold, while **P1** only exhibited a 2.9-fold emission enhancement at 590 nm. This has been ascribed to different sensitivity of excited state of the two iridium(III) complexes to polarity, which was supported by the fact that, compared to complex **Ir1**, complex **Ir2** displayed a higher dependence of the luminescence quantum yield and lifetime on the polarity of the solvent (Figure S2, Supporting Information).

Based on these findings, we incorporated both complexes into the same PNNPAM and synthesized a dual-emissive phosphorescent polymer (**P3**). Considering the different sensitivity of excited state of complexes to polarity and different reaction activity of complexes, the feed ratios listed in Table 1 were adopted to obtain appropriate ratiometric luminescence response. The photophysical properties of **P3** in phosphate buffer saline (PBS, pH = 7.4) at different temperatures were investigated. The results revealed that the phosphorescence intensity from **Ir2** at 470 nm was remarkably enhanced upon increasing temperature, while that from **Ir1** at 590 nm only exhibited a relatively moderate enhancement (Figure 2c), which was consistent with the temperature sensing performance of **P1** and **P2** and resulted in a ratiometric luminescence response; the intensity

Table 1. Physical properties of the phosphorescent polymers prepared in this study.

Polymers	Monomer ratio in feed[a)]	Yield/%	Composition in polymer[a)]	M_w[b)]	M_n[c)]	PDI (M_w/M_n)
P1	100: 2.67: 0.09: 0	36.3	100: 2.01: 0.15: 0	20500	11200	1.83
P2	100: 2.67: 0: 0.86	32.2	100: 2.36: 0: 0.85	21000	10300	2.03
P3	100: 2.67: 0.09: 0.86	30.7	100: 2.32: 0.11: 0.89	20700	10100	2.05

[a)]NNPAM: APTMA: **Ir1**: **Ir2**; [b)]Weight-average molecular weight; [c)]Number-average molecular weight.

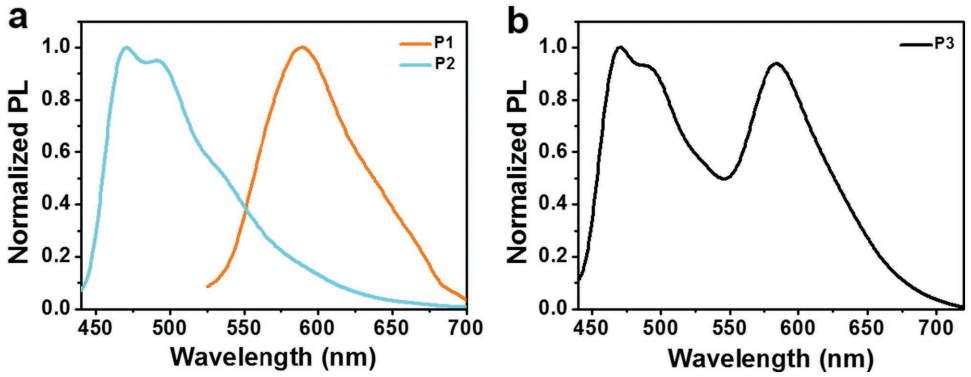

Figure 1. Normalized emission spectra of a) **P1** (orange), **P2** (cyan), and b) **P3** in phosphate buffer saline (pH = 7.4) at 25 °C.

ratio ($I_{470\ nm}/I_{590\ nm}$) increased by about 18.2-fold (Figure 2d) and the luminescence color of the **P3** solution changed from orange through white to cyan when temperature increased from 10 °C to 40 °C (Figure 2e). This luminescence color change has been attributed to the temperature-induced conformational response of **P3**. The transmission electron microscopy (TEM) images indicated that **P3** existed in spherical particles at 25 °C (Figure 2g). The dynamic light scattering (DLS) analysis revealed that the

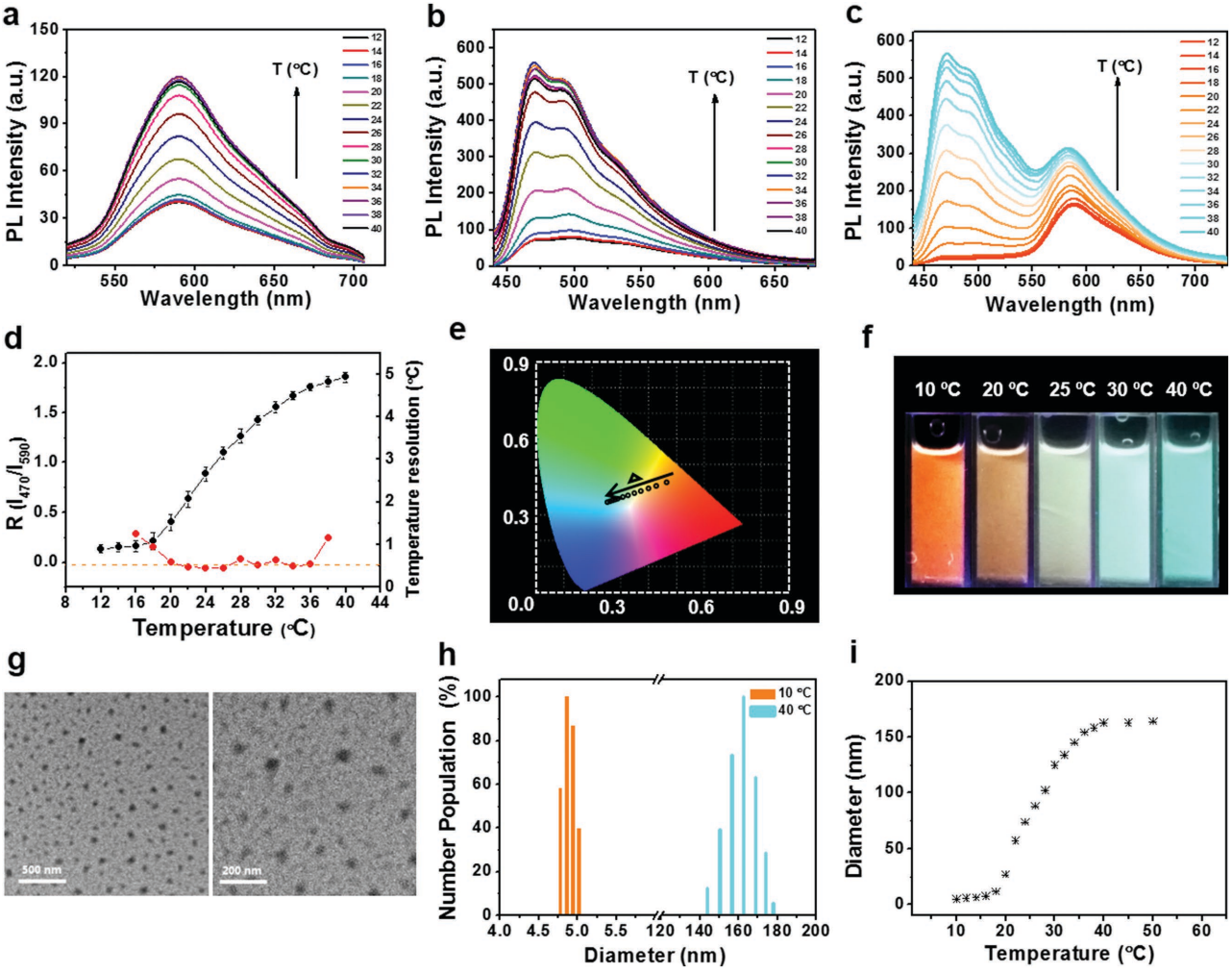

Figure 2. Emission spectra of a) **P1**, b) **P2**, and c) **P3** (0.01 w/v%) in phosphate buffer saline (pH = 7.4) at various temperatures; d) temperature-dependent ratio of phosphorescence intensity at 470 and 590 nm (black, left axis) and temperature resolution (red, right axis); e) CIE chromaticity diagram showing the temperature dependence of the (*x*, *y*) color coordinates; f) photographs of **P3** in aqueous solution at different temperatures; g) the transmission electron microscopy images of **P3**; h) the hydrodynamic diameters of **P3** (0.01 w/v%, 0.15×10^{-1} M KCl, pH = 7.4) at different temperatures; i) a correlation between the temperatures and the micelles sizes of the **P3** as examined by DLS measurements. Excitation wavelength was 405 nm.

Adv. Funct. Mater. **2016**,
DOI: 10.1002/adfm.201600706

hydrodynamic diameter of **P3** was reduced to 4.9 nm at 10 °C but increased to 162.8 nm at 40 °C (Figure 2h,i). At low temperature, **P3** showed good water solubility and dispersibility owing to hydrogen bonding between the amide linkages of **P3** and water molecules. Upon increasing temperature, the water molecules were released and hydrophobic interaction among **P3** led to partial aggregation and the microenvironment of the iridium(III) complexes was reduced in polarity and increased in rigidity. Hence, a sharp luminescence color change was observed (Figure 2f) with a high temperature resolution (about 0.4–0.6 °C) and a wide temperature functional range (Figure 2d).

The emission lifetime of **P3** at different temperature was also recorded via PLIM. **Figure 3**a showed that the photoluminescence lifetime (482 ± 35 nm) extended from 223.6 to 498.5 ns when the temperature was increased from 15 to 35 °C, while the photoluminescence lifetime (≥550 nm) got a moderate increase from 779.3 to 885.4 ns. Relative PLIM images of **P3** solution and corresponding phosphorescence decays were shown in Figure S3 (Supporting Information). Besides, considering that PLIM can provide spatially resolved luminescence lifetime data based on the photon arrival statistics at each pixel of the image, the change of **P3** solution states responsive to temperature was investigated.

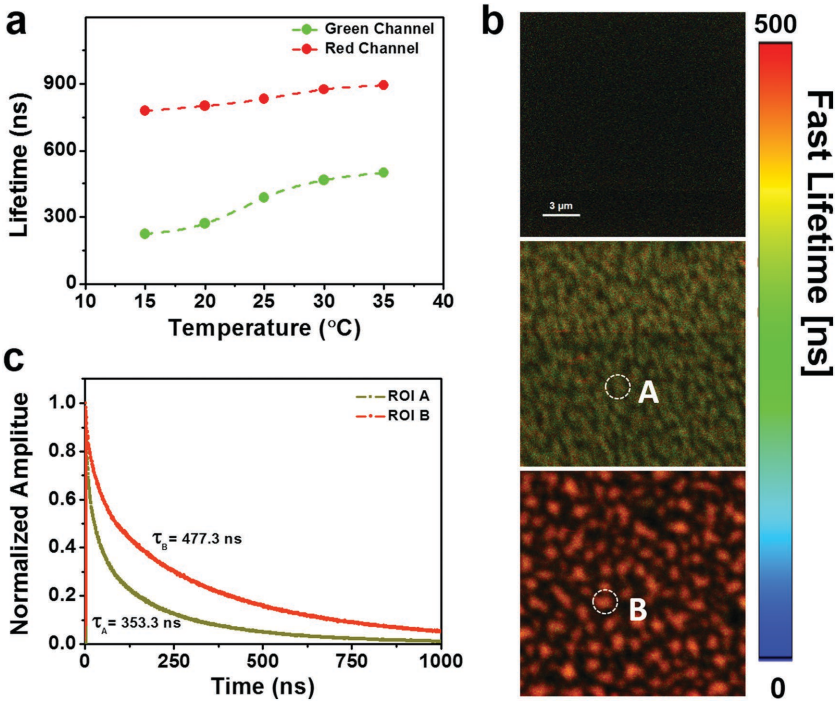

Figure 3. a) Luminescence lifetime versus temperature. The green channel was collected through bandpass filter (482 ± 35 nm); the red channel was collected through long-pass filter (≥550 nm). b) The PLIM images of **P3** solution at 15 °C (top), 25 °C (middle), and 35 °C (bottom); c) experimental luminescence decay curves of ROI A (25 °C) or ROI B (35 °C). τ was the average luminescence lifetime calculated from the double exponential decay fits. The luminescence at 15 °C was too weak to be calculated. Excitation wavelength was 405 nm.

As shown in Figure 3b, the highly magnified PLIM images of **P3** solution at different temperatures were shown, in which the photoluminescence through the bandpass filter (482 ± 35 nm) was collected for evaluating emission lifetime, since the cyan emission band of **P3** was more sensitive to temperature. At lower temperatures, **P3** solution is homogeneous. Then, the micelles gradually formed with increasing temperature. Along with the change of polymer conformation, the emission intensity and lifetime range of **P3** varied. As shown in Figure 3c, photoluminescence intensity collected at 15 °C was too weak to be analyzed, while ROI A and B at higher temperatures were selected for the detailed study. On average, ROI B was more than one order of magnitude brighter than ROI A, and displayed a wide distribution of photoluminescence lifetimes from 300 to 600 ns, while ROI A clearly shows a narrow distribution of lifetimes centered around 350 ns. Representative solution photoluminescence decays for ROI A and ROI B are fitted with exponential decay functions and the resulted lifetimes are 353.3 and 477.3 ns, respectively. Thus, the extended lifetime along with temperature-induced conformational response of polymers in microscale can be monitored via PLIM.

2.3. Evaluation of Potential Application of Polymer as Biological Probe

The potential application of **P3** for intracellular and in vivo temperature measurement has been evaluated. **Figure 4**a showed that the luminescence response of **P3** exhibited good reversibility when the temperature was changed between 15 and 35 °C repeatedly. The improvement of the reproducibility compared with the relative standard deviation (RSD) without ratiometry (Figure S4, Supporting Information) may be attributed to the signal of the single emission readout affected by some other factors, such as the distribution of the nanoparticles, power of excitation, and sensitivity of detectors. Figure 4b indicated good stability of **P3**; though the phosphorescence spectra displayed minor differences, the ratio ($I_{470\ nm}/I_{590\ nm}$) did not show notable change for the solution stored over 25 h. In addition, the solution of **P3** still possessed good reversibility even it had been stored more than three months.

Considering that the content of probe cannot be determined quantitatively in living cells and the environmental conditions in living cells, such as ionic strength, pH, and protein concentration are not constant in space and time, further investigation to verify the thermal responsive properties of **P3** in cell culture and the influence of the intracellular species has been conducted. The experiments demonstrated that the ratiometric phosphorescence response was independent of **P3** concentration (0.001–0.01 w/v%), pH values (4–10), and ionic strength of the solution (50–450 × 10^{-1} KCl), but slightly affected by protein concentrations (Figure S5, Supporting Information).

Photobleaching and cytotoxicity are other problems that limit the application of many luminescence probes in living organism. The cytotoxicity of **P3** toward HeLa cells was evaluated by the 3-(4,5-dimethyl-2-thiazolyl)-2,5-diphenyltetrazolium

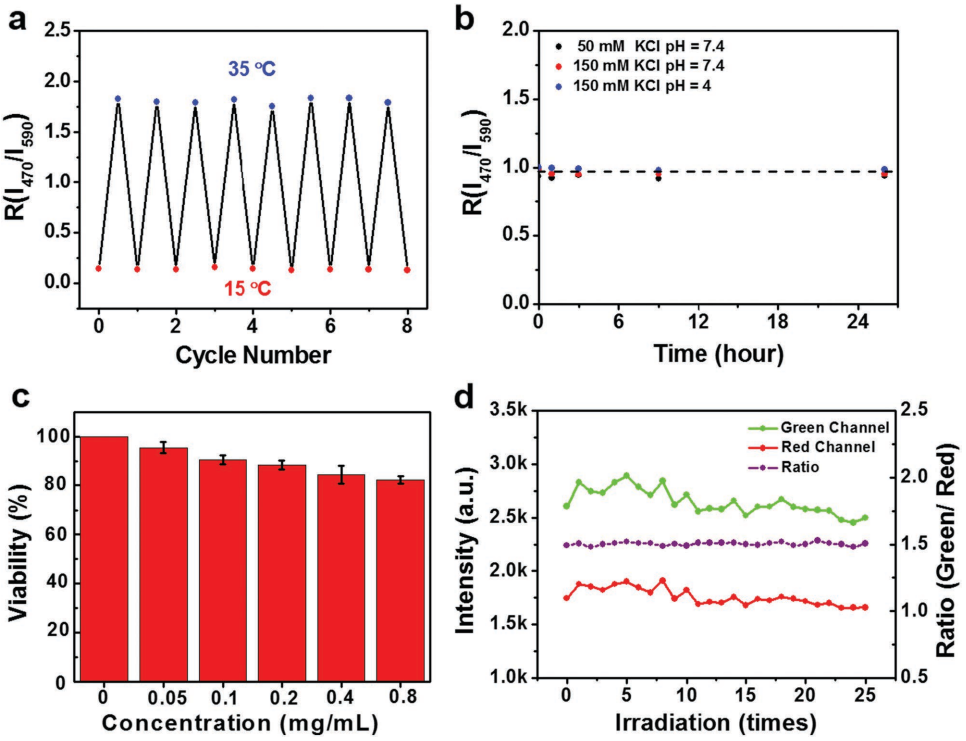

Figure 4. a) Reversibility of the phosphorescence response of **P3** (0.01 w/v%) to temperature variation in potassium chloride (150×10^{-1} M) solution (coefficient of variance (CV), 15 °C, CV% = 2.3%, 35 °C, CV% = 1.5%); b) stability of **P3** (0.01 w/v%) in potassium chloride solutions with different concentration and pH value at 25 °C for over 26 h; c) cytotoxicity of **P3** on HeLa cells determined by MTT assay; d) photostability of **P3** in living HeLa cells. Laser power: 100 μW; irradiation time: 15 s $scan^{-1}$; emission wavelength: 460–510 nm (green channel, green line, left axis) and 570–620 nm (red channel, red line, left axis); ratio of green and red fluorescence (blue line, right axis). Excitation wavelength was 405 nm.

bromide (MTT) assay.[18] **P3** had no obvious effects on the cell viability at a concentration less than 0.8 mg mL^{-1} (Figure 4c), which demonstrated its good biocompatibility. Figure 4d showed that both the green and red luminescence were photostable under the illumination of the laser at 405 nm with the power of 100 μW. Although a slight variation in luminescence intensity was observed due to the fluctuation in the excitation source power, it was well eliminated by using the luminescence intensity ratio of the green over the red luminescence.

2.4. Application of Polymer for Intracellular Temperature Sensing

The use of **P3** for intracellular temperature sensing was demonstrated via confocal laser scanning microscopy. The temperature of extracellular buffer was controlled using a heating stage and a digital thermocouple. The excitation wavelength was 405 nm and phosphorescence signals in the green (460–510 nm) and orange (570–620 nm) channels were collected. The experiment results exhibited that **P3** can be efficiently internalized by the endocytosis of HeLa cells. After co-incubation with **P3** in serum-free cell culture medium at ambient temperature for 2 h, appreciable amounts of **P3** were uptaken into the HeLa cells. As shown in **Figure 5**a, the phosphorescence intensity in the green channel increased with rising temperature, and that in the red channel changed slightly, which was consistent with the results observed in aqueous solution. The ratiometric luminescence imaging revealed that the phosphorescence ratio at the green channel to the red channel increased from 0.82 to 1.79 when the temperature was increased from 15 °C to 35 °C. The small difference of thermal sensitivity of **P3** between in solution and in cells may be arisen from inconsistency between PBS buffer solution and real environment, which can be negligible. To demonstrate the resistance of the ratiometric detection to external influences, other four different experimental conditions were controlled for ratiometric temperature imaging (Figure 5b and Figure S6, parts 4–8, Supporting Information): (4–6) the incubation concentration of **P3** was varied from 0.005 to 0.02 w/v%; (7) the incubation duration of **P3** was shorten to 1 h; (8) the 405 nm laser power was randomly increased. Different from the fluctuant intensity recorded in green or red channels, the ratios only depended on the temperature, and were independent of the dose of **P3**, incubation time, or power of excitation laser. Based on the strong resistance toward external influences, accurate intracellular temperature determination was achieved with ratiometric readout.

2.5. Application of Polymer for in vivo Temperature Sensing

Encouraged by the feasible temperature sensing in living cells, we subsequently examined the capability of **P3** in zebrafish larva (120 hpf), considering that zebrafish is widely used for studying vertebrate development and cancers.[19,20] As confocal images shown in **Figure 6**a, the luminescence distributes in the

DOI: 10.1002/adfm.201600706

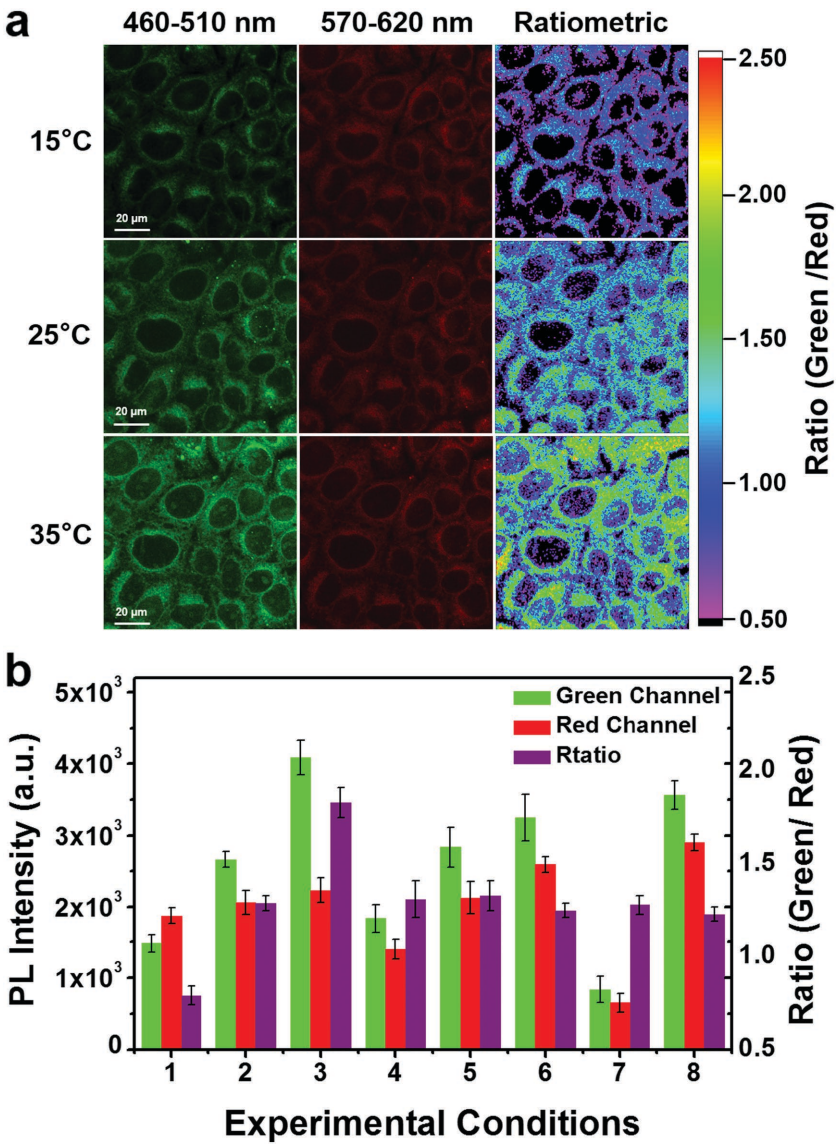

Figure 5. a) Confocal laser scanning microscopy images of HeLa cells labeled with **P3** at 15 °C (top), 25 °C (middle), and 35 °C (bottom). The green channels (left) were acquired by collecting the luminescence from 460 to 510 nm, while the red channels (center) were from 570 to 620 nm. The ratiometric luminescence images (right) were the green channel to red channel; b) luminescence intensity of HeLa cells recorded from the green channel (green) and the red channel (red) and the intensity ratio green/red (purple). (2), (3), (4) Luminescence intensity and ratio were collected from images in panel (a) (15, 25, and 35 °C). Control experimental conditions: images were collected at 25 °C. (4–6) the HeLa cells were treated with different concentration **P3** (0.005, 0.01, and 0.02 w/v%) for 2 h; (7) the time of incubation was shortened to 1 h; (8) the laser power was randomly increased. Excitation wavelength was 405 nm.

whole of zebrafish larva, and the luminescence intensity in yolk sac and belly was particularly strong. Upon increasing temperature, both the emission intensities of green channel (collected at wavelengths from 460 to 510 nm) and red channel exhibited slight increase. Additonally, the luminescence ratio of the green channel (collected at wavelengths from 460 to 510 nm) to the red channel (collected at wavelengths from 570 to 620 nm) did not display obvious increase when the temperature increased from 22 to 28 °C (Figure 6b). This phenomenon is probably due to the interference induced by the intense autofluorescence in vivo.

Nonetheless, we acquired a satisfactory result via the PLIM. As shown in Figure 6c, the PLIM images well distinguished the short-lived autofluorescence and the long-lived phosphorescence of **P3**, although the emission lifetime of **P3** was shorter than that in aqueous solution. By deducting the photons with lifetimes shorter than 150 ns, we eliminated the intense autofluorescence from the yolk sac and belly of the zebrafish. Importantly, similar to the variation trend in aqueous solution, the PLIM images showed that the phosphorescence lifetimes of **P3**, detected through the bandpass filter (482 ± 35 nm), increased from 321.3 to 447.5 ns when the temperature was increased from 22 to 28 °C; while the rise of the phosphorescence lifetimes detected through the bandpass filter (≥550 nm) was nearly negligible. This result demonstrated that the phosphorescent polymer probe exhibits an evident difference in emission lifetimes at different temperatures in complex physiological environmental, which could be clearly observed. Thus, the polymer can be applied as an excellent PLIM probe for sensing temperature in vivo.

To further demonstrate the ability of anti-interference when **P3** was applied for temperature sensing in vivo, the TGLI measurement has been carried out. In this experiment, the luminescence intensity images at different time ranges were collected from the bandpass filter (482 ± 35 nm) (Figure 6d). When the signal was collected at a time range of 0 to 2000 ns, the images of **P3**-treated zebrafish exhibited high signal intensities at two temperatures due to the presence of intense autofluorescence and **P3**. Once a particular time delay was exerted, such as the image collected at a time range of 150 to 2000 ns, the signal intensity of intense short-lived autofluorescence from the zebrafish could be eliminated effectively. Thus, the emission signal from **P3** could be observed, and the change of emission of **P3** at different temperatures (22 and 28 °C) can be monitored by TGLI. When further time delay was exerted (the image collected at a time range of 500 to 2000 ns), a larger difference of signal intensities between two temperatures appeared; at higher temperature (28 °C), the long-lived luminescence (τ_o > 500 ns) became stronger compared to that at lower temperature (22 °C), which indicated that temperature sensing becomes more sensitive by collecting the signal at a long time range via the TGLI technique. All these results indicated that **P3** can be used not only as intensity-based thermometer for ratiometric temperature determination

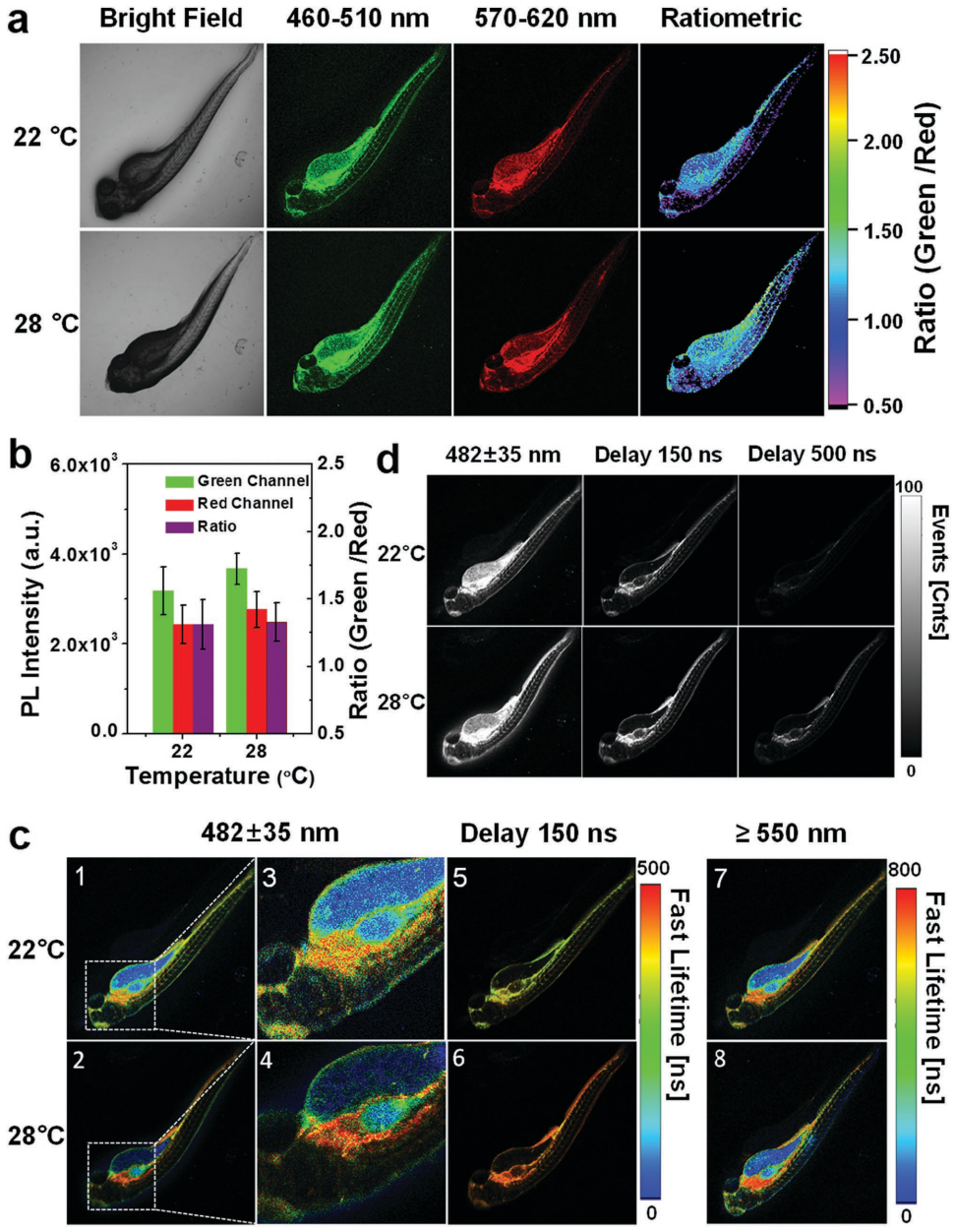

Figure 6. a) Bright images and confocal laser scanning microscopy images of living zebrafish larva after injection of **P3** at 22 °C (top) and 28 °C (bottom). The green channels were acquired by collecting the luminescence from 460 to 510 nm, while the red channels were from 570 to 620 nm. The ratiometric luminescence images (right) were the green channel to red channel. b) Luminescence intensity of zebrafish recorded from the green channel (green) and the red channel (red) and the intensity ratio (green/red) (purple) at 22 or 28 °C. c) PLIM images of living zebrafish larva at 22 and 28 °C. The lifetimes (482 ± 35 nm) were obtained with PL decay curve from 0–2000 ns (parts 1–4) and 150–2000 ns (parts 5, 6). The lifetimes (≥550 nm) were obtained with PL decay curve from 0–2000 ns (parts 7, 8). d) TGLI images of living zebrafish at 22 and 28 °C. The luminescence (482 ± 35 nm) was obtained with a delay of 0 ns (left), 150 ns (center), and 500 ns (right), respectively. Excitation wavelength was 405 nm.

in vitro, but as lifetime-based probe for temperature sensing in vivo.

3. Conclusion

In this work, we have developed a novel water-soluble dual-emissive phosphorescent polymeric thermometer that could be applied to temperature sensing in vitro and in vivo via ratiometric imaging and time-resolved luminescence imaging. The thermometer displayed good stability and biocompatibility. In particular, the ratiometric luminescence response improved the accuracy of the intracellular temperature mapping compared to intensity-based methods and the time-resolved luminescence imaging minimized the short-lived autofluorescence interference and improved signal-to-noise ratio. To the best of our knowledge, this is the first example of using luminescent probes for in vivo temperature sensing. In the future work,

Adv. Funct. Mater. **2016**,
DOI: 10.1002/adfm.201600706

efforts will be put on the improvement of the sensitivity of the probe and extension of the temperature mapping to mammals.

4. Experimental Section

General Experimental Information: All operations were performed under an inert nitrogen atmosphere using standard Schlenk unless otherwise stated. All solvents were used after distillation and stored over activated molecular sieves (5 Å). All reagents and chemicals were procured from commercial sources and used without further purification unless otherwise noted. All solvents were of analytical grade and purified according to standard procedures.[1] APTMA chloride was purchased from TCI. Cell culture reagents and fetal bovine serum (FBS) were purchased from Gibcco. The ^{1}H, ^{13}C, and ^{19}F NMR spectra were recorded on a Bruker Ultra Shield Plus 400 MHz NMR instrument at 298 K using deuterated solvents. Chemical shifts are given in ppm, and are referenced against external Me_4Si (^{1}H, ^{13}C). Mass spectra were obtained on a Bruker autoflex matrix-assisted laser desorption ionization time-of-flight (MALDI-TOF) mass spectrometer. The number-average molecular weight (M_n) and weight-average molecular weight (M_w) of the polymers were characterized in THF by GPC at 308 K (polystyrene as standard). TEM was conducted on a JEOL JEM-2100 transmission electron microscope at an acceleration voltage of 100 kV. Average particle size was measured via DLS on Zetasizer Nanoseries (Nano ZS90). The UV–vis absorption spectra were obtained with a Shimadzu UV-3600 UV–vis–NIR spectrophotometer. Photoluminescence spectra were measured on an Edinburgh FL 920 spectrophotometer equipped with a temperature controller. Excited-state lifetime studies were performed with an Edinburgh LFS-920 spectrometer with a hydrogen-filled excitation source. The data were analyzed by iterative convolution of the luminescence decay profile with the instrument response function using a software package provided by Edinburgh Instruments. The absolute quantum yields of the complexes were determined through an absolute method by employing an integrating sphere. The solution was degassed by three freeze-pump-thaw cycles. Photographs of the solution samples were taken with a Cannon EOC 400D digital camera under a hand-held UV lamp. Confocal luminescence imaging was carried out on an Olympus IX81 laser scanning confocal microscope with a stage plate heater (INUB-ONICS, Tokai Hit) and a thermocouple probe immersed in the solution. The PLIM setup was integrated with the same Olympus IX81 laser scanning confocal microscope. The lifetime values were calculated with professional software provided by PicoQuant Company.

*Synthesis of [Ir(pqa)$_2$(pap)]$^+PF_6^-$ (**Ir1**)*: A mixture of cyclometalated iridium(III) chloro-bridged dimer [Ir(pqa)$_2$Cl]$_2$ (500.0 mg, 0.26 mmol) and *N-(1,10-phenanthrolin-5-yl)propionamide* (160.0 mg, 0.64 mmol) in solution of dichloromethane/methanol (1:1 v/v) was heated at reflux under nitrogen for 6 h. The mixture was then cooled to room temperature, and KPF_6 (998 mg, 5.30 mmol) was added to the solution. Then, the mixture was evaporated under reduced pressure. Lastly, chromatography on silica gel with dichloromethane/acetone (30:1, v/v) as the eluent gave the orange-red complex **Ir1**. Yield: 53%. ^{1}H NMR (400 MHz, DMSO-d$_6$) δ (ppm): 10.17 (s, 1H), 9.23 (dd, J = 0.8 Hz, 8.8 Hz, 1H), 8.66 (dd, J = 1.2 Hz, 8.2 Hz, 1H), 8.56 (dd, J = 0.9 Hz, 4.8 Hz, 1H), 8.44 (dd, J = 1.2 Hz, 5.2 Hz, 1H), 8.34 (s, 2H), 8.11–7.96 (m, 8H), 7.64–7.60 (m, 2H), 7.22–7.18 (m, 2H), 6.97–6.76 (m, 24H), 6.54 (dt, J = 8.8Hz, 2.4 Hz, 2H), 6.04 (dd, J = 2.4 Hz, 4.8 Hz, 2H), 1.08 (t, J = 7.6 Hz, 3H). ^{13}C NMR (400 MHz, DMSO-d$_6$) δ (ppm): 169. 9, 164.8, 152.7, 152.4, 149.2, 148.9, 148.0, 147.1, 146.7, 145.8, 144.0, 139.6, 138.6, 138.0, 134.9, 133.5, 131.5, 130.8, 130.3, 129.6, 129.4, 129.0, 128.9, 127.6, 126.9, 126.8, 126.5, 126.3, 126.1, 124.8, 123.4, 123.3, 119.7, 117.9, 113.6, 50.01, 31.33. MALDI-TOF-MS *m/z*: 1185.94 [M-PF$_6^-$]$^+$.

*Synthesis of [Ir(fpp)$_2$(ppa)] (**Ir2**)*: A mixture of complex [Ir(fpp)$_2$(hpa)] (200.0 mg, 0.27 mmol), K_2CO_3 (100.0 mg, 0.72 mmol), and bromopropane (0.2 mL, 2.20 mmol) was added to *N,N*-dimethylformamide (15 mL). The mixture was stirred under nitrogen at 25 °C for 12 h. After cooling, the organic phase was concentrated and then purified by silica gel chromatograph using dichloromethane/ethyl acetate (5:1, v/v) to give the lawn green complex **Ir2**. Yield: 75%. ^{1}H NMR (400 MHz, DMSO-d$_6$) δ (ppm): 8.56 (dd, J = 0.8Hz, 5.6 Hz, 1H), 8.24 (dd, J = 8.0 Hz, 18.4 Hz, 2H), 8.07–7.98 (m, 2H), 7.78 (dd, J = 0.8 Hz, 8.8 Hz, 1H), 7.64 (dd, J = 0.8 Hz, 6.0 Hz, 1H), 7.52–7.47 (m, 2H), 7.34–7.30 (m, 1H), 7.26 (dd, J = 0.8 Hz, 4.8 Hz, 1H), 6.84–6.73 (m, 2H), 5.65 (dd, J = 2.4 Hz, 8.4 Hz, 1H), 5.43 (dd, J = 2.4 Hz, 8.8 Hz), 4.03 (t, J = 6.4 Hz, 2H), 1.74 (m, 2H), 0.99 (t, J = 7.2 Hz, 3H). ^{13}C NMR (400 MHz, DMSO-d6) δ (ppm): 170.46, 164.12 (d,J = 7.0 Hz), 163.50 (d,J = 6.8 Hz), 163.18 (dd,J = 12.8 Hz, 253 Hz), 162.67 (dd, J = 12.3 Hz, 256 Hz), 161.15 (dd, J = 13.4 Hz, 257.5 Hz), 160.83 (dd, J = 12.9 Hz, 257.4 Hz), 159.06, 155.15 (d, J = 60 Hz), 154.15 (d, J = 6.2 Hz), 149.43, 148.46, 140.72, 139.76 (d, J = 7.2 Hz), 138.31, 130.58, 128.57 (t, J = 3.4 Hz), 128.34 (t, J = 3.4 Hz), 125.03, 124.44, 124.01, 123.20 (dd, J = 8.5 Hz, 19.3 Hz), 114.12 (t, J = 9 Hz), 98.09 (t, J = 27.0 Hz), 97.93 (t, J = 27.0 Hz), 70.73, 22.36, 10. 85. ^{19}F NMR (376 MHz, DMSO-d$_6$) δ (ppm): –107.66 (d, J = 10.2 Hz), –108.48 (d, J = 9.8 Hz), –109.68 (d, J = 10.2 Hz), –110.25 (d, J = 10.2 Hz). MALDI-TOF-MS *m/z*: 753.36.

The detailed synthesis of complexes and relative ligands can be found in the Supporting Information.

*Synthesis of **P1**, **P2**, and **P3***: A mixture of PNNPAM (352.0 mg, 3.1 mmol), APTMA chloride (25μL, 82.8 μmol), 2,2-azobisisobutyronitrile (5.5 mg, 33.5 μmol), complex **Ir3** (3.0 mg, 2.25 μmol), and complex **Ir4** (20.0 mg, 26.6 μmol) was dissolved in *N,N*-dimethylformamide (3.0 mL). The solution was bubbled with dry nitrogen for 2 h to remove dissolved oxygen and then stirred under nitrogen at 80 °C for 12 h. After cooling, the reaction mixture was poured into diethyl ether (250.0 mL), and the obtained **P3** was purified by reprecipitation using methanol/diethyl ether (5 ml/250 mL) and dialysis. Yield: 30.7%. GPC (THF, polystyrene standard): M_n = 10 100, PDI = 2.05. For the preparation of **P1**, the complex **Ir3** (3 mg, 2.25 μmol) was added to the above mixture and other procedure was same. Yield: 36.3%. GPC (THF, polystyrene standard): M_n = 11 200, PDI = 1.83. For the preparation of **P2**, the complex **Ir4** (20 mg, 26.6 μmol) was added to the above mixture and other procedure was same. Yield: 32.2%. GPC (THF, polystyrene standard): M_n = 10 300, PDI = 2.03. The contents of the NNPAM and APTMA units in the copolymers were determined from Bruker Ultra Shield Plus 400 MHz NMR instrument. The proportions of the iridium(III) complexes units in the copolymers were determined from their absorbance in dichloromethane with the model iridium(III) complexes (**Ir1**, ε = 12 400 M^{-1} cm^{-1} at 400 nm, ε = 9100 M^{-1} cm^{-1} at 500 nm; **Ir2**, ε = 2000 M^{-1} cm^{-1} at 400 nm).

Cell Culture and MTT Assay: HeLa cells were cultured in Dulbecco's modified eagle medium (DMEM) supplemented with 10% FBS, 100 U of penicillin, and 100 μg mL^{-1} streptomycin in a humidified incubator at 37 °C and 5% CO_2. The in vitro cytotoxicity toward HeLa was measured using the methyl thiazolyl tetrazolium (MTT, Beyotime) assay. Briefly, cells growing in log phase were seeded into 96-well cell culture plate at 1×10^4 per well. **P3** was added to the wells of the treatment group at concentrations of 0.05, 0.1, 0.2, 0.4, and 0.8 mg mL^{-1}. The cells were incubated for 24 h at 25 °C under 5% CO_2. The MTT (5 mg mL^{-1}) in PBS solution was added to each well, and incubated for another 4 h. After removal of the culture solution, 200 μL DMSO was added to each well, shaking for 10 min at shaking table. An enzyme-linked immunosorbent assay reader (BioTek Instruments, Rower Wave XS2) was used to measure the OD570 (Absorbance value) of each well referenced at 570 nm. The following formula was used to calculate the viability of cell growth:

$$\text{Viability (\%)} = \begin{pmatrix} \text{mean of absorbance value of treatment group/} \\ \text{mean of absorbance value of control} \end{pmatrix} \times 100$$

Luminescence Imaging: HeLa cells used for imaging were first incubated in culture dishes until their adherence. The cells were washed with PBS three times and then incubated with **P3** 0.01 w/v% in in serum-free DMEM for 2 h at 25 °C and 5% CO_2. Cell imaging experiments were then performed after the cells were washed and covered with 1 mL

PBS in the culture dishes for imaging. The zebrafish larvae (120 hpf) were purchased from Model Animal Research Center of Nanjing University. All the zebrafish larvae experiments were carried out in accordance with the relevant laws and the guidelines of Institutional Animal Care and Use Committee. Femtojet (Eppendorf) controlled by a micromanipulator (Eppendorf) was used for microinjection. **P3** was dissolved in an aqueous solution (1 w/v%) and the solution was filtered using an Ultrafree-MC (Millipore) and microinjected into the zebrafish with a glass capillary needle Femtotips II (Eppendorf). The volume of the injected solution was estimated to be 1 pL.

Luminescence imaging was performed with an Olympus IX81 laser scanning confocal microscope, a 40 × objective lens for cells and a 4 × objective lens for zebrafish. Organisms containing the **P3** were excited at 405 nm with a semiconductor laser, and the emission was measured according to the spectral data. The images were accomplished using the software package provided by Olympus instruments. After each temperature change, we waited for about 15 min before starting a new measurement to ensure thermal equilibration.

PLIM and TGLI techniques were adopted on the platform afforded by Olympus IX81 laser scanning confocal microscope and PicoQuant Company. The objective lens was 40× and the frequency was 0.5 MHz for **P3**. Phosphorescence was excited with 405 nm light, the emission was collected through a bandpass filter (482 ± 35 nm). The correlative calculations of the data were carried out with the software provided by PicoQuant.

Calibration Curve and Temperature Resolution: The calibration curve for thermometry with **P3** was obtained by approximating the relationship between averaged ratio of phosphorescence intensity at 470 and 590 nm ($n = 9$) and temperature to the sextuple polynomial (with Microsoft Excel 2010, $R^2 = 0.9999$, 16 °C< T <38 °C, Equation (1))

$$R(T) = 2.4966\times10^{-9}T^6 - 2.2065\times10^{-6}T^5 + 2.9628\times10^{-4}T^4 - 1.6756\times10^{-2}T^3 + 0.4709T^2 - 6.3780T + 33.1449 \quad (1)$$

where T and R (T) represent temperature in Celsius and ratio of phosphorescence intensity at 470 nm and 590 nm at T °C, respectively.

The temperature resolution[5a] (δT) of DDPT can be generally evaluated by using Equation (2).

$$\delta T = \left(\frac{\partial T}{\partial R}\right)\delta R \quad (2)$$

where $\partial T/\partial R$ and δR represent the inverse of the slope in the ratio–temperature diagram and the standard deviation of the ratio of phosphorescence intensity, respectively.

In this system, $\partial T/\partial R$ was obtained by differentiating the polynomial $R(T)$ (Equation (1)) and δR was calculated with the following Equation (3) as the averaged difference between $R(T)$ and the ratio of phosphorescence intensity experimentally acquired

$$\delta R = \frac{\sum_i^n |R_i(T) - R(T)|}{n} \quad (3)$$

where n and $R_i(T)$ imply the test number and the ratio of phosphorescence intensity at T °C, respectively.

Supporting Information

Supporting Information is available from the Wiley Online Library or from the author.

Acknowledgements

This work was supported by the National Basic Research Program of China (2012CB933301), National Natural Science Foundation of China (51473078 and 21504040), Natural Science Foundation of Jiangsu Province of China (BM2012010), Synergetic Innovation Center for Organic Electronics and Information Displays, Scientific and Technological Innovation Teams of Colleges and Universities in Jiangsu Province (TJ215006), and Priority Academic Program Development of Jiangsu Higher Education Institutions (YX03001).

Received: February 7, 2016
Revised: February 24, 2016
Published online:

[1] a) B. B. Lowell, B. M. Spiegelman, *Nature* **2000**, *404*, 652; b) A. Bahat, I. Tur-Kaspa, A. Gakamsky, L. C. Giojalas, H. Breitbart, M. Eisenbach, *Nat. Med.* **2003**, *9*, 149; c) D. A. Warner, R. Shine, *Nature* **2008**, *451*, 566; d) C. E. Holleley, D. O'Meally, S. D. Sarre, J. A. Graves, T. Ezaz, K. Matsubara, B. Azad, X. Zhang, A. Georges, *Nature* **2015**, *523*, 79.

[2] a) M. Monti, L. Brandt, J. Ikomi-Kumm, H. Olsson, *Scand. J. Haematol.* **1986**, *36*, 353; b) R. J. DeBerardinis, J. J. Lum, G. Hatzivassiliou, C. B. Thompson, *Cell Metab.* **2008**, *7*, 11; c) T. Vreugdenburg, C. Willis, L. Mundy, J. Hiller, *Breast Cancer Res. Treat.* **2013**, *137*, 665.

[3] K. M. McCabe, M. Hernandez, *Pediatr. Res.* **2010**, *67*, 469.

[4] a) Y. Y. Chen, A. W. Wood, *Bioelectromagnetics* **2009**, *30*, 583; b) S. Arai, S.-C. Lee, D. Zhai, M. Suzuki, Y. T. Chang, *Sci. Rep.* **2014**, *4*, 6701; c) M. Homma, Y. Takei, A. Murata, T. Inoue, S. Takeoka, *Chem. Commun.* **2015**, *51*, 6194.

[5] a) C. Gota, K. Okabe, T. Funatsu, Y. Harada, S. Uchiyama, *J. Am. Chem. Soc.* **2009**, *131*, 2766; b) K. Okabe, N. Inada, C. Gota, Y. Harada, T. Funatsu, S. Uchiyama, *Nat. Commun.* **2012**, *3*, 705; c) T. Tsuji, S. Yoshida, A. Yoshida, S. Uchiyama, *Anal. Chem.* **2013**, *85*, 9815. d) J. Qiao, C. Chen, L. Qi, M. Liu, P. Dong, Q. Jiang, X. Yang, X. Mu, L. Mao, *J. Mater. Chem. B* **2014**, *2*, 7544; e) S. Uchiyama, T. Tsuji, K. Ikado, A. Yoshida, K. Kawamoto, T. Hayashic, N. Inadac, *Analyst* **2015**, *140*, 4498; f) J. Liu, X. Guo, R. Hu, J. Xu, S. Wang, S. Li, Y. Li, G. Yang, *Anal. Chem.* **2015**, *87*, 3694.

[6] A. E. Albers, E. M. Chan, P. M. McBride, C. M. Ajo-Franklin, B. E. Cohen, B. A. Helms, *J. Am. Chem. Soc.* **2012**, *134*, 9565.

[7] L. Shang, F. Stockmar, N. Azadfar, G. U. Nienhaus, *Angew. Chem., Int. Ed.* **2013**, *52*, 11154.

[8] a) F. Vetrone, R. Naccache, A. Zamarron, A. Juarranz de la Fuente, F. Sanz-Rodriguez, L. Martinez Maestro, E. Martin Rodriguez, D. Jaque, J. Garcia Sole, J. A. Capobianco, *ACS Nano* **2010**, *4*, 3254; b) L. H. Fischer, G. S. Harms, O. S. Wolfbeis, *Angew. Chem., Int. Ed.* **2011**, *50*, 4546; c) L. H. Fischer, G. S. Harms, O. S. Wolfbeis, *Angew. Chem.* **2011**, *50*, 4640.

[9] a) J. S. Donner, S. A. Thompson, M. P. Kreuzer, G. Baffou, R. Quidant, *Nano Lett.* **2012**, *12*, 2107; b) S. Kiyonaka, T. Kajimoto, R. Sakaguchi, D. Shinmi, M. Omatsu-Kanbe, H. Matsuura, H. Imamura, T. Yoshizaki, I. Hamachi, T. Morii, Y. Mori, *Nat. Methods* **2013**, *10*, 1232.

[10] a) F. Ye, C. Wu, Y. Jin, Y.-H. Chan, X. Zhang, D. T. Chiu, *J. Am. Chem. Soc.* **2011**, *133*, 8146; b) G. Ke, C. Wang, Y. Ge, N. Zheng, Z. Zhu, C. J. Yang, *J. Am. Chem. Soc.* **2012**, *134*, 18908.

[11] X. Wang, O. S. Wolfbeis, R. J. Meier, *Chem. Soc. Rev.* **2013**, *42*, 7834.

[12] Y. Takei, S. Arai, A. Murata, M. Takabayashi, K. Oyama, S. Ishiwata, S. Takeoka, M. Suzuki, *ACS Nano* **2014**, *8*, 198.

[13] a) S. W. Botchway, M. Charnley, J. W. Haycock, A. W. Parker, D. L. Rochester, J. A. Weinstein, J. A. G. Williams, *Proc. Natl. Acad. Sci. USA* **2008**, *105*, 16071; b) Y. You, Y. Han, Y.-M. Lee, S. Y. Park, W. Nam, S. J. Lippard, *J. Am. Chem. Soc.* **2011**, *133*, 11488; c) T. V. Esipova, A. Karagodov, J. Miller, D. F. Wilson, T. M. Busch, S. A. Vinogradov, *Anal. Chem.* **2011**, *83*, 8756;

d) H. Woo, S. Cho, Y. Han, W.-S. Chae, D.-R. Ahn, Y. You, W. Nam, *J. Am. Chem. Soc.* **2013**, *135*, 4771; e) H. Sun, S. Liu, W. Lin, K. Y. Zhang, W. Lv, X. Huang, F. Huo, H. Yang, G. Jenkins, Q. Zhao, W. Huang, *Nat. Commun.* **2014**, *5*, 3601; f) E. Baggaley, M. R. Gill, N. H. Green, D. Turton, I. V. Sazanovich, S. W. Botchway, C. Smythe, J. W. Haycock, J. A. Weinstein, J. A. Thomas, *Angew. Chem., Int. Ed.* **2014**, *53*, 3367; g) E. Baggaley, S. W. Botchway, J. W. Haycock, H. Morris, I. V. Sazanovich, J. A. Gareth Williams, J. A. Weinstein, *Chem. Sci.* **2014**, *5*, 879; h) E. Roussakis, J. A. Spencer, C. P. Lin, S. A. Vinogradov, *Anal. Chem.* **2014**, *86*, 5937; i) D. Aigner, R. I. Dmitriev, S. M. Borisov, D. B. Papkovsky, I. Klimant, *J. Mater. Chem. B* **2014**, *2*, 6792; j) E. Baggaley, I. V. Sazanovich, J. A. Gareth Williams, J. W. Haycock, S. W. Botchwayd, J. A. Weinstein, *RSC Adv.* **2014**, *4*, 35003; k) R. I. Dmitriev, S. M. Borisov, H. Düssmann, S. Sun, B. J. Müller, J. Prehn, V. P. Baklaushev, I. Klimant, D. B. Papkovsky, *ACS Nano* **2015**, *9*, 5275.

[14] a) J. Huang, T. Watanabe, K. Ueno, Y. Yang, *Adv. Mater.* **2007**, *19*, 739; b) V. Fernández-Moreira, F. L. Thorp-Greenwood, M. P. Coogan, *Chem. Commun.* **2010**, *46*, 186; c) D.-L. Ma, H.-Z. He, K.-H. Leung, D. S.-H. Chan, C.-H. Leung, *Angew. Chem., Int. Ed.* **2013**, *52*, 7666; d) L. Lu, D. S.-H. Chan, D. W. J. Kwong, H.-Z. He, C.-H. Leung, D.-L. Ma, *Chem. Sci.* **2014**, *5*, 4561; e) D.-L. Ma, D. S.-H. Chan, C.-H. Leung, *Acc. Chem. Res.* **2014**, *47*, 3614; f) M. Mauro, A. Aliprandi, D. Septiadi, N. S. Kehra, L. De Cola, *Chem. Soc. Rev.* **2014**, *43*, 4144; g) K.-H. Leung, H.-Z. He, B. He, H.-J. Zhong, S. Lin, Y.-T. Wang, D.-L. Ma, C.-H. Leung, *Chem. Sci.* **2015**, *6*, 2166; h) K. Y. Zhang, J. Zhang, Y. Liu, S. Liu, P. Zhang, Q. Zhao, Y. Tang, W. Huang, *Chem. Sci.* **2015**, *6*, 301; i) Q. Zhao, X. Zhou, T. Cao, K. Y. Zhang, L. Yang, S. Liu, H. Liang, H. Yang, F. Li, W. Huang, *Chem. Sci.* **2015**, *6*, 1825; j) M. Wang, Z. Mao, T.-S. Kang, C.-Y. Wong, J.-L. Mergny, C.-H. Leung, D.-L. Ma, *Chem. Sci.* **2016**, DOI: 10.1039/C6SC00001K.

[15] a) S. Ito, *Kobunshi Ronbunshu* **1989**, *46*, 437; b) S. Uchiyama, Y. Matsumura, A. Prasanna de Silva, K. Iwai, *Anal. Chem.* **2003**, *85*, 5926; c) C. Gota, S. Uchiyama, T. Ohwada, *Analyst* **2007**, *132*, 121.

[16] a) Y. Hu, G. Zhang, R. P. Thummel, *Org. Lett.* **2003**, *5*, 2251; b) K. Nonoyama, *Bull. Chem. Soc. Jpn.* **1974**, *47*, 467; c) S. Sprouse, K. A. King, P. J. Spellane, R. J. Watts, *J. Am. Chem. Soc.* **1984**, *106*, 6647; d) Y. Ohsawa, S. Sprouse, K. A. King, M. K. DeArmond, K. W. Hanck, R. J. Watts, *J. Phys. Chem.* **1987**, *91*, 1047; e) T.-H. Kwon, M. K. Kim, J. Kwon, D. Y. Shin, S.-J. Park, C.-L. Lee, J.-J. Kim, J.-I. Hong, *Chem. Mater.* **2007**, *19*, 3673.

[17] H. G. Schild, *Prog. Polym. Sci.* **1992**, *17*, 163.

[18] T. Mosmann, *J. Immunol. Methods* **1983**, *65*, 55.

[19] a) W. Drieve, D. Stemple, A. Schie, L. Solnica-Krezel, *Trends Genet.* **1994**, *10*, 152; b) D. J. Grunwald, J. S. Eisen, *Nat. Rev. Genet.* **2002**, *3*, 717

[20] a) J. F. Amatruda, J. L. Shepard, H. M. Stern, L. I. Zon, *Cancer Cell* **2002**, *1*, 229; b) H. M. Stern, L. I. Zon, *Nat. Rev. Cancer* **2003**, *3*, 533; c) S. Liu, S. D. Leach, *Annu. Rev. Pathol.: Mech. Dis.* **2011**, *6*, 71.